JOURNAL OF PROPULSION AND POWER
Vol. 25, No. 2, March–April 2009

High-Pressure Supercritical Turbulent Cryogenic Injection and Combustion: A Single-Phase Flow Modeling Proposal

François-Xavier Demoulin*
Université de Rouen, 76801 Saint Etienne du Rouvray, France
Stephan Zurbach†
Société Nationale d'Etude et de Construction de Moteurs d'Aviation, 27208 Vernon, France
and
Arnaud Mura‡
Ecole Nationale Supérieure de Mécanique et d'Aérotechnique, 86961 Futuroscope France

DOI: 10.2514/1.36948

Despite recent progress, the complex geometry of rocket engine combustion chambers with several hundreds of injectors and the multifaceted physical processes involved in supercritical conditions still remain difficult to handle by using direct numerical simulation or even large eddy simulation methodologies. Accordingly, with a target of performing the simulation of practical configurations, a hierarchy of Reynolds-averaged Navier–Stokes closures is developed and studied herein. Following the conclusions of previous experimental investigations, including supercritical conditions, mixing, and subsequent chemical reaction between LOx and GH2, the modeling proposals rely on the infinitely-fast-chemistry hypothesis. Within this framework, special care is required to model the turbulent mixing phenomena because they control the whole combustion process. In the supercritical conditions under consideration, turbulent mixing processes are expected to lie between 1) mixing in gaseous conditions (because surface-tension effects and latent heat of vaporization do not hold above the critical point) and 2) mixing between a gas phase and a liquid phase (because the density variations are very important and are comparable with those encountered in two-phase flows). Three different modeling proposals to represent these specific features associated with supercritical mixing are applied to the calculation of a reference cryogenic turbulent jet flame.

I. Introduction

IN ROCKET engine applications, the description of the turbulent mixing between liquid oxygen (LOx) and gaseous hydrogen (GH2) at elevated pressures and the accurate representation of the subsequent turbulent combustion processes still remain challenging issues [1]. Considering the Reynolds-averaged Navier–Stokes (RANS) framework, the expected modeling difficulty concerns mainly the physical processes taking place just downstream of the injector exit, where the LOx concentration values are very high. With a very few exceptions [2,3], most of the previous works on this subject assume that the LOx jet is directly atomized by the high-velocity coflowing stream of hydrogen to produce a spray of LOx droplets, and classical Lagrangian models are applied. However, by using such a Lagrangian description, the initial zone of jet fragmentation is difficult to handle and must be modeled by calibrating inlet conditions, just to recover the experimental trends.

The corresponding primary breakup zone consists of a turbulent mixture of liquid and gas in which it is quite difficult to distinguish between well-defined droplets (or blobs) of liquid and surrounding gas. This is especially true when supercritical conditions are considered, because the stabilizing effect of surface tension tends to disappear at very high working pressures. Nevertheless, it must be recognized that the poor description of the primary breakup zone is a relatively common shortcoming of two-phase flow models, whatever the operative pressures. However, in the situation under consideration (i.e., LOx–GH2 combustion at elevated pressures), the primary breakup phenomenon plays an essential role.

Accordingly, additional modeling efforts are necessary to deal with the description of the corresponding part of the flow, because the fragmentation of the jet of heavy fluid and the combustion processes is strongly coupled [4]. First steps in this direction have been reported in [3,4], which have been more recently followed by the study of Jay et al. [2], in which a combined surface-density approach for both 1) the surface that separates the heavy fluid (HF) from the light fluid (LF) and 2) the flame has been put forward to describe dense spray combustion. Compared with these studies, the work of Demoulin et al. [5], devoted to the description of two-phase flows of liquid and gas, focuses on the description of the turbulent liquid mass flux, a quantity that is expected to play a significant role to describe the atomization process, because it determines the level of liquid turbulent dispersion. Indeed, the majority of atomization models are mainly focused on the spray granulometry, but the most important parameter is, above all, the liquid concentration in terms of either the liquid volume or the liquid mass fraction. This is especially true when reactive two-phase flows are considered, because the global equivalence ratio, including both vaporized and liquid fuel, is determined by the liquid-dispersion process.

With respect to previous studies, the aim of the present work is to evaluate the relative influence of some of the different physical phenomena that need to be modeled when describing LOx–GH2 combustion in supercritical conditions such as those encountered in rocket engine applications. The analysis is performed within a RANS framework, because the complexity of the corresponding geometries, which contain several hundreds of injectors, still remains out of reach for large eddy simulation (LES) calculations. Nevertheless, significant progress has been made in this direction when considering a single injector element, and the latter approach has recently allowed deeper insights into such complex turbulent reactive flows [6–8].

Received 1 February 2008; revision received 17 October 2008; accepted for publication 20 October 2008.

*Complexe de Recherche Interprofessionnel en Aérothermochimie, Unité Mixte de Recherche 6614, Centre National de la Recherche Scientifique, Site Universitaire du Madrillet, B.P. 12.

†SAFRAN Group, Space Engines Division, Forêt de Vernon, B.P. 802.

‡Laboratoire de Combustion et de Détonique, Unité Propre de Recherche 9028, Centre National de la Recherche Scientifique, Téléport 2-1, Avenue Clément Ader, B.P. 40109; arnaud.mura@lcd.ensma.fr (Corresponding Author).

Furthermore, it is noteworthy that one of the problems associated with the RANS approach is that it can only recover the large-scale structure. More details concerning such applications of LES to supercritical mixing and combustion can be found, for instance, in [8] and references within. If the classical principles of thermodynamics can be applied directly to obtain density and transport coefficients that describe the supercritical state within the direct numerical simulation (DNS) framework [9–11], the situation is quite different within either RANS or LES frameworks, because only averaged or filtered values are available. The absence of any further consideration for this peculiarity can lead to serious misinterpretations, simply because the laws of thermodynamics that relate the different quantities do not rely on linear relationships.

In the present study, we have chosen to restrict the scope of our investigations to three particular facets of supercritical reactive mixtures and to build three corresponding possible RANS models. The first aspect (and associated modeling proposal) only accounts for the disappearance of a proper interface between the two phases at elevated pressures. Accordingly, if we except the peculiar density evolution considered in the following (which results from the consideration of the Benedict–Webb–Rubin equation of state), the approach retained to describe LOx and GH2 combustion mainly gathers the characteristics of gas mixtures, and the corresponding strategy is denoted as the gas–gas (GG) model.

The second specific aspect is related to the high value of the density ratio between LOx and GH2. This is a typical feature encountered in two-phase flows of liquid and gas; accordingly, the GG model is then modified to represent some of the corresponding peculiarities associated with liquid–gas mixtures, especially those associated with turbulent mixing. The resulting proposal is denoted as the light-fluid—heavy-fluid (LF-HF) model.

Finally, a transport equation for the mean surface density is introduced to focus on the persistence of high-density-gradient magnitude (HDGM) layers that have been evidenced through DNS studies performed in supercritical conditions . This specific feature is taken into account by supplementing the LF-HF model with a modeled transport equation for the mean surface density Σ, and the resulting model is denoted as LF-HF-Σ. The results obtained with the different modeling proposals are compared to discriminate what particular aspect prevails, to improve the final output of a RANS simulation. The conclusions are drawn from a direct comparison with a well-documented experimental test case of LOx–GH2 combustion in supercritical conditions.

The three main facets on which attention is focused through a specific modeling proposal are first briefly described in the next section. The rest of the manuscript is organized as follows: in Sec. III, the turbulent flux of the mixture-fraction variable that represents the initial fuel dispersion is discussed in the context of flows with strongly variable density. Previous results obtained for turbulent liquid fluxes in two-phase flows are extended to the consideration of supercritical conditions in which mixtures are made up of LF and HF. Section IV is devoted to the general formulation of the presumed probability density function (PDF) model in the infinitely-fast-chemistry limit that incorporates real-gas effects; accordingly, the generic equations of the model are presented and the experimental test case retained for validation is also described. In Sec. V, the results obtained by using the GG formulation are presented. All of the necessary developments of the model to incorporate the effects induced by the presence of HF and LF are then introduced, and the results obtained using the corresponding approach, called LF-HF, are compared with the reference experiment. The equation for the surface density Σ and the comparison between the results obtained with the LF-HF-Σ model and the experiments are described in Sec. VII. Finally, the generality of both modeling proposals and conclusions drawn from the previous sections are assessed through a complimentary comparison with another set of experimental data.

II. Description of the Different Modeling Proposals

A. GG Model

Because of the high levels of operative pressure, the proper liquid–gas interface may vanish in such a manner that the surface-tension effects or the latent heat of vaporization do not hold anymore. In these conditions, oxygen behaves like some kind of heavy gas: molecular diffusion takes place at small scales, resulting in the mixing of the oxygen with the surrounding gaseous hydrogen at the molecular level. Assuming that turbulent mixing and combustion take place as in common gaseous turbulent reactive flows, standard closures can be applied (in particular, to describe turbulent transport and small-scale mixing rates.

The turbulent scalar fluctuations are likely to have a deep impact on the description of the combustion process, and a classical presumed PDF framework is retained here to take them into account. For the present test case, the reactants H2 and O2 are considered, and it seems reasonable to assume that the chemical equilibrium is reached. This modeling assumption is supported by previous experimental investigations [1] that did not evidence any special signs of finite rate chemistry influence. A detailed chemical description is then retained to obtain realistic flame temperature and species concentrations. The influence of chemistry and real-gas effects and their fluctuations on the flowfield is taken into account through the mean density evaluation. Because this model is, in essence, very similar to a gas–gas description of combustion, it is denoted as GG in the following.

B. LF-HF Model

This second modeling attempt extends the previous approach (namely, the GG model) by taking into account the influence of the high density difference that exists between the two phases. Indeed, the density changes can reach more than 2 orders of magnitude from the light GH2 stream to the heavy LOx stream. Strong density gradients exist and are only slowly dissipated through molecular diffusion and conduction. The occurrence of the corresponding HDGM layers has been already evidenced by direct numerical simulation analysis [11–13].

As a direct consequence of the persistence of such high density gradients, the considered mixture is expected to display some similarities with two-phase flows even above the critical point, with the densest stream being assimilated to a liquid and the lightest to a gas. However, because the surface-tension influence becomes all the more vanishingly small as the pressure is increased, it does not require any further consideration as supercritical conditions are reached, and the turbulent mixing that takes place between LOx and GH2 gathers some essential features of an atomizing two-phase flow, but in the limit of infinite Weber number values. The closure proposed in [5] has been specifically designed for this limiting behavior, but it requires further modifications to describe supercritical conditions. In particular, the representation of molecular mixing at small scales is a special issue that must be addressed.

In comparison with two-phase flows of liquid and gas that were previously considered in [5], the situation is much more complex and must be considered with a new formalism; in particular, a new variable is introduced: namely, the Reynolds-averaged value of the Favre fluctuation (RAFF) of the mixture fraction. This special variable quantifies the level of density fluctuations that ranges from zero for a flow without density variations to unity in the limit of an infinite level of density difference between the two streams. Consistent with the first modeling proposal (i.e., the GG model), the presumed PDF framework is kept to represent turbulent combustion, but the modified turbulent mixing law of [5] is incorporated as the first step of extension toward supercritical conditions. The considered presumed PDF shape is still based on the Beta PDF shape, but it is modified to describe the dense part of the flow.

Finally, one important difference between low pressure and supercritical conditions concerns the local mass transfer. In the subcritical case, it is governed by droplet evaporation, whereas it is inadequate at elevated pressures above the critical point. The consideration of this special issue raises important modifications in

the closure of the transport equation of the mixture-fraction variance, especially for the scalar-dissipation-rate modeling. Because all of these modifications aim at extending the GG model to make it able to describe specific features encountered in supercritical mixtures of LF and HF, it is denoted as LF-HF in the following.

C. LF-HF-Σ Model

The third proposal concerns the possible improvement that can be obtained through the consideration of a surface separating the LF from the HF. Such a surface obviously exists in liquid–gas flows. In this case, it has been clearly established [2,14,15] that there is an interest in considering the mean surface density of the liquid–gas interface to improve the description of certain terms such as, for instance, the total vaporization rate, which is directly related to the available amount of interface. Even if it seems worthless at first to stay interested in the mean surface density of such an interface that is vanishing in supercritical conditions, recent studies have established that such a quantity can still be defined and useful to describe turbulent mixing [2,13,16]. In the supercritical case, the surface cannot be defined as the place at which the liquid-vapor equilibrium may exist, but it can be viewed as an isosurface that is associated with a certain level of local mixing. For supercritical flows close to the critical state, there still exists the HDGM layer, as discussed previously.

Okong'o and Bellan [13] suggested that the surface that separates HF from LF can be characterized by the HDGM layer, and they studied the production and destruction rates of the corresponding surface area using DNS results. In an attempt to improve the description of the corresponding small-scale processes, the second modeling proposal is modified to incorporate a mean surface-density transport equation for the boundary surface that separates the heavy fluid from the light fluid. Then the mass transfer per unit of this boundary surface is introduced. Because this modeling proposal extends the previous closure by considering a mean surface-density equation, it is called LF-HF-Σ, where Σ denotes the mean surface density in terms of its area per unit of volume.

Having introduced the basic principles of the different modeling strategies (i.e., GG, LF-HF, and LF-HF-Σ), it seems appropriate to propose a hierarchy of models that successively includes each of the corresponding characteristics and to test and validate each of them in a well-documented experiment. In the following, the model retained to describe turbulent combustion is the classical presumed PDF approach with tabulated chemical equilibrium. Within such an infinitely-fast-chemistry framework, the key points rely on the following:

1) The closure of the turbulent scalar fluxes describes the mixing of the species at large scale.

2) The retained presumed PDF shape describes the small-scale features of the flow.

3) The scalar dissipation rate drives the relaxation of the PDF toward homogeneous conditions.

Accordingly, the presumed PDF approach is first used and described in the context of the GG approach. The LF-HF model is introduced in the second step. It is based on the GG model, but considering that some similarities associated with high density ratio can be expected between the LOx–GH2 mixtures under consideration and high-Weber-number two-phase flows, the PDF shape and closures of both turbulent transport and scalar dissipation rate are modified. The corresponding models are described before testing the LF-HF model. Finally, a modeled transport equation for the mean surface density is considered to improve the description of the mass-transfer rate between the two phases and the corresponding contribution to the scalar dissipation rate. The resulting LF-HF-Σ model is discussed before testing it on the same set of experimental data.

III. Turbulent Scalar Fluxes in Variable-Density Flows: From Two-Phase Flows to Supercritical Conditions

A key issue to describe turbulent mixing in multicomponent reactive mixtures is to model the turbulent fluxes of each species. When LOx–GH2 mixtures are considered, specific physical phenomena induced by the large density variations are expected to come into play. In the following, a dedicated model is described; it relies on a previous study devoted to the modeling of liquid–gas (water–air) situations that also display such large density variations. This previous work is first briefly recalled and the strategy retained for liquid–gas situations is extended to the consideration of LOx–GH2 mixtures.

In a recent study reported in [5], the approach introduced in [4,14,17–20], which is based on a turbulent mixing framework to describe the atomization process, has been successfully modified to improve the description of the liquid-dispersion process. In this representation, the turbulent two-phase flow downstream of the injector exit is viewed as a single turbulent mixture in which liquid and gas are considered as two different species, both described with an Eulerian point of view. The closure relies on a *liquid indicator*: that is, a quantity that measures the mean liquid mass fraction $\tilde{Y}_l$, which is unity in the liquid phase and zero in the gas phase. This quantity is also often denoted as the phase indicator or phase function [2], and it allows elegant derivations of the Eulerian balance equations that describe two-phase flows and their subsequent averaging [21]. The flowfield is characterized through a single mean velocity together with a turbulence model for variable-density flows. In [5], different models of turbulence have been tested, from the conventional k-ϵ model to the full second-order methodology. The obtained results have emphasized the critical role of the turbulent flux of liquid. In fact, as outlined in [14], the specific features of this Eulerian representation, and especially the use of a single mean velocity $\tilde{u}_i$, to describe the whole mixture do not necessarily imply that liquid and gas have the same mean velocity. Actually, the slip velocity between the two phases is directly related to the turbulent liquid mass flux through the following exact equation:

$$\overline{\rho u_i'' Y_l''} = \bar{\rho}\tilde{Y}_l\tilde{Y}_g(\bar{u}_{l,i} - \bar{u}_{g,i}) = \bar{\rho}\tilde{Y}_l(\bar{u}_{l,i} - \tilde{u}_i) \tag{1}$$

where u_i'' is the fluctuating velocity field, and $\tilde{Y}_l$, $\tilde{Y}_g$, $\bar{u}_{l,i}$, and $\bar{u}_{g,i}$ are, respectively, the liquid mass fraction, the gas mass fraction, and the mean velocities, respectively, conditioned in the liquid and in the gas phase. Note that the Reynolds average and fluctuations

$$\phi = \bar{\phi} + \phi' \quad \text{with} \quad \bar{\phi}' = 0 \tag{2}$$

will be used in conjunction with the Favre average and fluctuations

$$\phi = \tilde{\phi} + \phi'' \quad \text{with} \quad \tilde{\phi} = \frac{\overline{\rho\phi}}{\bar{\rho}} \tag{3}$$

throughout the whole paper, and some of the different bridges existing between the two formalisms should be kept in mind:

$$\tilde{\phi} = \bar{\phi} + \frac{\overline{\rho'\phi'}}{\bar{\rho}} \quad \text{and} \quad \overline{\phi''} = -\frac{\overline{\rho'\phi'}}{\bar{\rho}} \tag{4}$$

Equation (1) underlines the relevance of our efforts to improve the modeling of the turbulent liquid mass flux, because the slip velocity can be sustained through inertial effects.

In the first step, atomization in nonreactive two-phase flow media of liquid and gas has been considered. The experimental investigation of the turbulent mass flux and of the initial liquid dispersion is more easily studied by using liquid water instead of LOx and air instead of GH2. Such experimental studies have been carried out, for instance, by Carreau et al. [22] and by Stepowski and Werquin [23] for different values of the momentum flux ratio between liquid and gas streams, also known as the J-number. These experimental results have been used as databases to test different modeling proposals [18,19]. One of the main conclusions of these preliminary studies is that the standard turbulent diffusivity approximation is clearly not sufficient to recover the experimental trends. Accordingly, a second-order modeling analysis has been carried out and the following correction for the turbulent transport law has been put forward [5]:

$$-\overline{\rho u_i'' Y_l''} = \bar{\rho}\left(\frac{\nu_T}{\mathrm{Sc}_{\tilde{Y}_l}} + C_\rho \frac{k^2}{\epsilon}\overline{\rho}\left(\frac{1}{\rho_g}-\frac{1}{\rho_l}\right)\tilde{Y}_l(1-\tilde{Y}_l)\right)\frac{\partial \tilde{Y}_l}{\partial x_i}$$

$$\text{with} \quad \nu_T = C_\mu \frac{k^2}{\epsilon} \tag{5}$$

where the modeling constant $C_\rho = 1.8$ has been retained after the analysis reported in [5]. With this generalized law, the turbulent diffusion approximation that is widely used to represent turbulent transport terms now appears with a correction factor that involves the density ratio between liquid and gas. In comparison with the classical turbulent diffusivity approximation, the appearance of this correction factor can be explained by the Rayleigh–Taylor instability [5]. Indeed, strong density variations combined with fluctuations of acceleration are known to promote the emergence of such a Rayleigh–Taylor instability in liquid–gas coflowing jets [24–26]. A direct consequence is the production of ligaments that project liquid blobs far away from the coflowing jet, thus enhancing the turbulent mixing efficiency. From a more practical point of view, the modeling proposal, as given by Eq. (5), can be easily implemented into a numerical computational fluid dynamics (CFD) code because it does not modify the form of the advective–diffusive scalar transport equation. This correction disappears if either only liquid or only gas is present. Finally, this simple algebraic correction has been found to improve the representation of the liquid dispersion in a very significant manner [5].

For the situation of a gaseous mixture with strong density differences, important effects such as those related to the Rayleigh–Taylor instability will compete with the dissipation of the density gradient layer, which is itself at the origins of the inertial effects. As a consequence, it is necessary to consider an additional quantity that is able to measure the result of this competition and the associated level of density variations. The quantity retained here is the RAFF $\overline{Y_l''}$, for which the exact definition is given by

$$\overline{Y_l''} = \bar{\rho}\int (Y_l - \tilde{Y}_l)\frac{\tilde{P}(Y_l)}{\rho}\mathrm{d}Y_l \tag{6}$$

where $\tilde{P}(Y_l)$ is the mass-weighted PDF of the liquid mass fraction Y_l. Clearly, the quantity $\overline{Y_l''}$ is not zero, because it is the Reynolds average of a Favre fluctuation. When mixtures made of liquid and gas are considered, the liquid mass fraction PDF is two-delta-peaked

$$\tilde{P}(Y_l) = (1-\tilde{Y}_l)\delta(Y_l) + \tilde{Y}_l\delta(Y_l - 1)$$

in such a manner that Eq. (6) becomes

$$\overline{Y_l''} = \bar{\rho}\left(\frac{1}{\rho_g}-\frac{1}{\rho_l}\right)\tilde{Y}_l(1-\tilde{Y}_l) \tag{7}$$

Hence, the RAFF corresponds exactly to the correction factor that appears in Eq. (5) and that was previously introduced in [5].

To go beyond the restrictive scope of the nonreactive two-phase flows previously considered, and to deal with nonpremixed combustion, a normalized mixture fraction Z is now introduced. This mixture-fraction variable ranges from unity in pure hydrogen (the liquid mass fraction being zero: that is, $\tilde{Y}_l = 0$) to zero in pure LOx (the liquid mass fraction being unity: that is, $\tilde{Y}_l = 1$). The simplest definition of the mixture fraction is as follows:

$$Z = \frac{Y_{\mathrm{H2}} + r_s(1 - Y_{\mathrm{O2}})}{1 + r_s} \tag{8}$$

where r_s is the mass stoichiometric ratio defined by

$$r_s = \frac{\nu_{\mathrm{O2}} W_{\mathrm{O2}}}{\nu_{\mathrm{H2}} W_{\mathrm{H2}}}$$

and W_i and ν_i are, respectively, the molecular weight of the ith species and the stoichiometric coefficient of the global reaction:

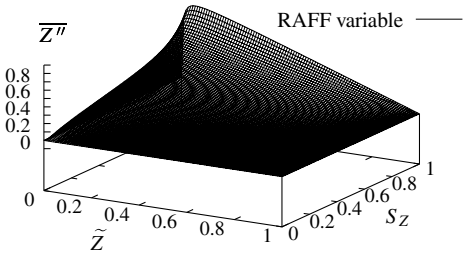

Fig. 1 Fluctuation level as a function of the average value and segregation rate of the mixture fraction for a LOx–GH2 mixture.

$$\nu_{\mathrm{H2}}\mathrm{H2} + \nu_{\mathrm{O2}}\mathrm{O2} \rightarrow \nu_{\mathrm{H2O}}\mathrm{H2O}$$

From the previous definition, the generalized law for the turbulent flux is extended to the consideration of the mixture-fraction variable according to

$$-\overline{\rho u_i'' Z''} = \bar{\rho}\left(\frac{\nu_T}{\mathrm{Sc}_{\tilde{Z}}} + C_\rho \frac{k^2}{\epsilon}|\overline{Z''}|\right)\frac{\partial \tilde{Z}}{\partial x_i} \tag{9}$$

The previous relationship is strictly equivalent to Eq. (5), written for a liquid–gas mixture, but it is more general and applicable to describe supercritical turbulent mixing between liquid oxygen and gaseous hydrogen. Indeed, the increase of the turbulent mass flux results from the density fluctuations that can be measured using the absolute value of $\overline{Z''}$. The latter value is easily obtained from the knowledge of the density $\rho(Z)$ and the probability density function $\tilde{P}(Z)$:

$$\overline{Z''} = \overline{Z - \tilde{Z}} = \overline{\rho\frac{(Z-\tilde{Z})}{\rho}} = \bar{\rho}\left(\frac{Z-\tilde{Z}}{\rho}\right) = \bar{\rho}\int_0^1 \frac{(Z-\tilde{Z})}{\rho(Z)}\tilde{P}(Z)\mathrm{d}Z \tag{10}$$

As already stressed for $\overline{Y_l''}$, the mixture-fraction RAFF vanishes in the absence of density variations, because Favre and Reynolds averages are equivalent in this case. In contrast, $\overline{Z''}$ is maximum if no mixing takes place at small scales, as expected for turbulent liquid–gas flows, and the maximum value tends toward unity as the density ratio tends to infinity.

Figure 1 shows the variations of $\overline{Z''}$ as a function of mixture-fraction average $\tilde{Z}$ and segregation rate $S_Z = \widetilde{Z''^2}/\tilde{Z}(1-\tilde{Z})$ for a LOx–GH2 mixture. Without any fluctuation, $\overline{Z''}$ is strictly equal to zero, but it can reach values close to unity for the present conditions, in which the density value ranges from about 6 kg/m^3 in the GH2 stream to more than 1200 kg/m^3 in the pure LOx stream.

IV. Turbulent Combustion of Hydrogen and Oxygen in Supercritical Conditions: Infinitely-Fast-Chemistry Closure

Because we are considering combustion between hydrogen and oxygen, the use of the classical fast-chemistry hypothesis does not appear as a restrictive choice, and the standard presumed mixture-fraction PDF approach is retained in conjunction with a chemical equilibrium library. Moreover, because supercritical conditions are investigated in the present study, the density is tabulated including real-gas effects. Figure 2 displays the corresponding density of a LOx–GH2 mixture as a function of the mixture fraction. This figure gives the density dependency as obtained from a Benedict–Webb–Rubin equation of state for the conditions described in the forthcoming sections of the paper and also summarized in Table 1. Further details concerning the special features related to the thermophysical properties of fluids at elevated pressures using this specific law of state can be found in [28]. The mixture evolution, depicted in Fig. 2, is as follows. In the oxidizer stream, the mixture is only made up of cold dense oxygen and the value of the density is very high. As the mixture fraction increases toward the conditions of the gaseous hydrogen stream, the density decreases abruptly but continuously to reach a value characteristic of an ideal gas.

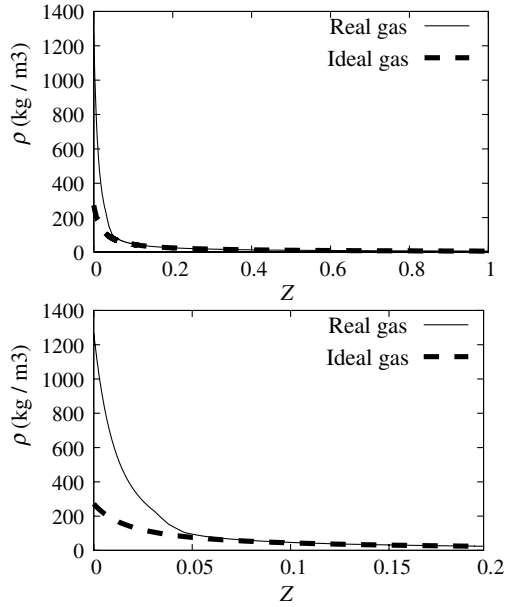

Fig. 2 Density of a LOx–GH2 mixture as a function of mixture fraction: ideal-gas and real-gas equation of state.

Finally, the mixture-fraction PDF $\tilde{P}(Z)$ that appears in Eq. (10) is first presumed with a standard Beta-function shape determined through the knowledge of its first two moments (i.e., the mean and variance values $\tilde{Z}$ and $\widetilde{Z''^2}$). The PDF shape can be estimated at each point of the computational mesh using the algorithms from the Numerical Recipes library [29]. The hydrogen–oxygen combustion is described through the detailed chemical kinetics mechanism proposed by Eklund et al. [30] involving 6 species. The chemical equilibrium state, which depends only on the equivalence ratio (or mixture fraction), at least for the given operating pressure and temperature in each reactant stream, is evaluated by using the CHEMKIN-II chemical kinetics code package [31]. The computations we carried out give the values of temperature $T^{\mathrm{eq}}(Z)$ and species mass fractions $Y_i^{\mathrm{eq}}(Z)$ at chemical equilibrium for different values of the composition variable Z, and to save computational time, the mean values of the different variables of interest are tabulated as functions of both mean mixture fraction $\tilde{Z}$ and segregation rate $S_Z = \widetilde{Z''^2}/\tilde{Z}(1-\tilde{Z})$ values.

The set of modeled equations is implemented into the FLUENT commercial CFD code [32] by using user-defined functions. In addition to the mean chemical composition, the mean density is tabulated as a function of mixture-fraction average and segregation rate, and the set of transport equations for mixture-fraction mean and variance are

$$\frac{\partial \bar{\rho}\tilde{Z}}{\partial t} + \frac{\partial \bar{\rho}\tilde{u}_j\tilde{Z}}{\partial x_j} = -\frac{\partial \overline{\rho u_j'' Z''}}{\partial x_j} \tag{11}$$

$$\frac{\partial \bar{\rho}\widetilde{Z''^2}}{\partial t} + \frac{\partial \bar{\rho}\tilde{u}_j\widetilde{Z''^2}}{\partial x_j} = -\frac{\partial \overline{\rho u_j'' Z''^2}}{\partial x_j} - 2\overline{\rho u_j'' Z''}\frac{\partial \tilde{Z}}{\partial x_j} - 2\bar{\rho}\epsilon_Z \tag{12}$$

Table 1 Input conditions for the RCM2 test case Mascotte single injector; $P = 60$ bar [27]

	GH2	LOx
Pressure, MPa	6	6
Temperature, K	287	85
Velocity, m/s	236	4.35

In the previous set of equations, the laminar diffusion terms have been discarded with respect to the turbulent ones, as expected for large-Reynolds-number turbulent flows.

The right-hand side (RHS) of Eq. (11) is closed by using the modified turbulent flux law of Eq. (9). The unclosed terms in the RHS of Eq. (12) are the turbulent transport of the scalar-variance field and the mean scalar dissipation term. The first is closed with the modified turbulent diffusion law:

$$-\overline{\rho u_j'' Z''^2} = \bar{\rho}\left(\frac{\nu_T}{Sc_{\tilde{Z}''^2}} + C_\rho \frac{k^2}{\epsilon}|\overline{Z''}|\right)\frac{\partial \widetilde{Z''^2}}{\partial x_j} \tag{13}$$

Following the previous analysis of [5], the value $C_\rho = 1.8$ is retained in Eqs. (9) and (13); note that the classical turbulent diffusivity closure is simply recovered by setting $C_\rho = 0.0$. The turbulent Schmidt numbers that appear in Eqs. (9) and (13) are set to their usual values: namely, $Sc_{\tilde{Z}} = Sc_{\tilde{Z}''^2} = 0.7$. The mean dissipation term is closed by using a standard linear relaxation model for the scalar-fluctuation decay rate:

$$\bar{\rho}\epsilon_Z = \overline{\rho D \frac{\partial Z''}{\partial x_j}\frac{\partial Z''}{\partial x_j}} = C_Z \bar{\rho}\frac{\epsilon}{k}\widetilde{Z''^2} \tag{14}$$

Other possibilities that rely on a modeled transport equation for the mean scalar dissipation rate have been discussed, for instance, in [33–35]. In Eq. (14), the turbulent-to-scalar time-scale ratio is supposed to be constant and equal to its usual value $C_Z = 2$. Finally, the turbulent flowfield is described with a one-point two-equation model, and the realizable k-ϵ has been retained [32].

The next step of the analysis consists of testing the different modeling proposals against experimental results. Unfortunately, the choice of available reference data to validate such a model for supercritical LOx–GH2 combustion is relatively scarce. Here, the Mascotte setup of ONERA has been retained as an experimental test case [36]. The corresponding test rig consists of a low-speed round LOx jet surrounded by an atomizing high-speed annular GH2 coflow. A large amount of data have been gathered in this experimental setup by different research teams from ONERA and Centre National de la Recherche Scientifique. The corresponding studies have been supported by Centre National d'Etudes Spatiales and Société Nationale d'Etude et de Construction de Moteurs d'Aviation in the framework of the Groupement de Recherche sur la combustion dans les Moteurs Fusées in France. Different measurements have been performed, but very few are at supercritical pressures and, in these conditions, the experimental database is essentially made of direct emission images of OH* radicals. Different fields of OH* emission have been obtained: the first type is the direct emission that issues from the optical path through the entire flame and the second is an Abel inverted image that estimates the OH* emission field in the center plane. Note that only excited OH* are obtained from experiments, whereas the whole contribution of OH radicals is considered in the numerical results. Experimental investigations have confirmed that the momentum flux ratio J between hydrogen and oxygen streams [i.e., $J = (\rho_{\mathrm{H2}}u_{\mathrm{H2}}^2)/(\rho_{\mathrm{O2}}u_{\mathrm{O2}}^2)$] is one of the key parameters for the flame structure because it drives the jet disintegration [37]. The first part of the present numerical study is focused on the experimental test cases that have been conducted with a value of $J = 11$.

V. Infinitely-Fast-Chemistry Model with Standard Turbulent Diffusivity Approximation: The GG Model

As already mentioned in the Introduction, the surface tension and latent heat of vaporization disappear in supercritical conditions, and the simplest approach consists of considering both propellant streams of LOx and GH2 as two gaseous streams and using standard models. Nevertheless, some of the peculiarities of the real fluids must be taken into account. Considering the Mascotte test rig as a significant step in this direction has been previously done by Cheng and Farmer [38]. In their study, the authors addressed the peculiarities of real-fluid effects through their linearized real-fluid-

model approach that accounts for phase changes through a generalized equation of state used to compute the thermal properties. Nevertheless, note that the numerical simulations of Cheng and Farmer ignore the influence of the turbulence on both transport and small-scale molecular mixing. Despite this simplification, the obtained results are realistic, even if they are not in fully satisfactory agreement with the experimental data.

In the first step of the present analysis, we propose to carry out computations similar to those previously performed by Cheng and Farmer in [38,39], in the sense that the influence we can expect from supercritical conditions on both turbulent transport and mass-transfer rate between the two phases is not specifically addressed. However, it is noteworthy that the present computations also slightly differ from those already performed by Cheng and Farmer [38]:

1) A simpler representation of real-gas effects is retained through the consideration of $\rho(Z)$ only.

2) The influence of turbulence on both scalar and velocity fields is taken into account.

Indeed, a standard single-point closure is retained to predict the turbulent velocity field, and the influence of scalar fluctuations is taken into account through the consideration of the mixture-fraction PDF $\tilde{P}(Z)$.

To this purpose, the previous set of equations (9–14) is considered, except that the turbulent transport terms are modeled by using the classical gradient-law approximation [that is, without taking the effects of density fluctuations into account: namely, by setting $C_\rho = 0$ in Eqs. (9) and (13)]. The input conditions for the considered Mascotte experiment labeled RCM3 (single injector at an operating pressure of 60 bar) are described in [27] and are also reported in Table 1. Figure 3 shows a comparison of the OH concentration field computed with the purely gaseous model: namely, by setting the value $C_\rho = 0$. This modeling proposal is referred to as the GG model in the following. From a qualitative point of view, the shape of the computed flame is in satisfactory agreement with the experimental visualizations, thus confirming the relevance of the infinitely-fast-chemistry assumption for such kinds of conditions. Nevertheless, the length of the simulated flame appears to be overestimated in comparison with experiments.

In previous works [5,18], it has been evidenced that incorporating the high density fluctuations effects into turbulent transport modeling can induce strong reductions of the mixing-core length. It is then expected that this closure may also significantly improve the present simulation; this is the subject of the next section.

VI. Similarity with Large Weber Number Atomizing Two-Phase Flows: The LF-HF Model

In addition to the studies that have evidenced the persistence of HDGM layers [11–13], simple test cases focused on the evolution of a density profile at high, low, and intermediate temperatures and in a large range of pressure conditions have also established that very different behaviors can be found, ranging from the pure-liquid vaporizing-droplet evolution to the classical diffusion process occurring between two ideal gases [40,41]. The initial density gradient can either be smoothed very quickly, a situation that corresponds to the diffusion between two different gases for which the density ratio is not too far from unity, or it is sustained and persistent up to the latest mixing stages, as with a vaporizing liquid (as expected for large density differences between the two fluids).

In the present case, the ratio of LOx to GH2 density is very large, and because of the gas expansion induced by exothermic chemical reactions, the difference is even more pronounced for the reactive than for the nonreactive case. Because density variations are very large, density gradients are likely to persist. The heavy fluid is disintegrated by turbulent motions into smaller and smaller parcels, but the resulting blobs have a longer lifetime than the usual pockets of gas, because the large density difference slows down the homogenization process at small scales. In other words, these blobs are not dissipated at a standard (i.e., gaseous) dissipation rate and, as expected, more attention should be paid to the closure of this quantity to improve the representation of the turbulent diffusion flame.

Considering Fig. 2, it seems convenient to divide the supercritical mixture into two distinct components: 1) a heavy fluid, also denoted as HF in the following, and 2) a light fluid for mixture fractions above a critical value Z_c, denoted as LF in the following. Here, the critical value $Z_c = 0.001$ has been retained from the consideration of the density evolution reported in Fig. 2. At the corresponding transition $Z = Z_c$, the mixing is likely to be reduced due to strong density differences between the two fluids and associated persistence of the HDGM layers.

A presumed PDF approach is used to describe the supercritical mixture distribution. For the sake of simplicity, a single Dirac delta peak positioned at $Z = 0$ is considered to represent the statistics below $Z = Z_c$. The final results should not be very sensitive to the choice of this particular value, because no significant chemical reaction may occur for the corresponding compositions. A Beta-function PDF is retained to represent fluid particles with a mixture-fraction value larger than Z_c. For this purpose, a normalized variable φ is introduced to describe the LF mixture:

$$\varphi = \frac{Z - Z_c}{1 - Z_c}$$

The corresponding PDF is schematically depicted in Fig. 4.

Finally, the mixture-fraction PDF is presumed with a Beta function:

$$\tilde{P}(Z) = \tilde{Y}_{\mathrm{HF}}\delta(Z) + \frac{\tilde{Y}_{\mathrm{LF}}}{1 - Z_c}\tilde{P}_\varphi(\varphi) \tag{15}$$

where the PDF that describes the LF mixture is given by

$$\tilde{P}_\varphi(\varphi) = \beta(\tilde{\varphi}|_{\mathrm{LF}}, \tilde{R}_\varphi|_{\mathrm{LF}})$$

with

$$\tilde{\varphi}|_{\mathrm{LF}} = \overline{\rho\varphi}|_{\mathrm{LF}}/\bar{\rho}|_{\mathrm{LF}} \quad \text{and} \quad \tilde{R}_\varphi|_{\mathrm{LF}} = \overline{\rho\varphi''^2}|_{\mathrm{LF}}/\bar{\rho}|_{\mathrm{LF}}$$

where $.|_{\mathrm{LF}}$ denotes a conditional average in the gas: namely, the LF phase.

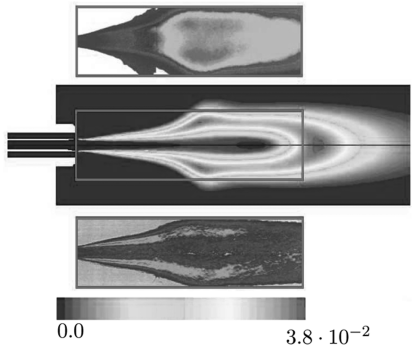

Fig. 3 Calculated OH concentration field obtained with the GG model [i.e., $C_\rho = 0$ in Eqs. (9) and (13)] and experimental OH* emission fields; direct emission (top) and Abel inverted image (bottom) [1,2,45,46].

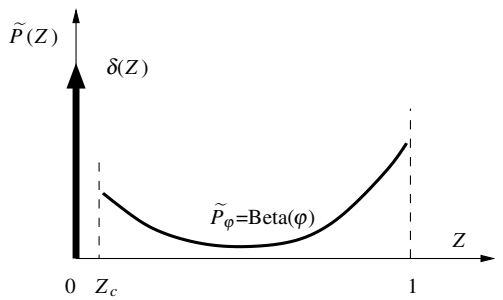

Fig. 4 Mixture-fraction PDF shape considered for supercritical conditions with large density fluctuations.

An additional transport equation for $\tilde{Y}_{\mathrm{LF}}$ (i.e., the mean value of the LF mass fraction) is considered. In this equation, the mass-transfer rate w_m quantifies the mass flux that crosses the isosurface $Z = Z_c$, defined to be positive when directed toward the LF phase:

$$\frac{\partial \bar{\rho}\tilde{Y}_{\mathrm{LF}}}{\partial t} + \frac{\partial \bar{\rho}\tilde{u}_j\tilde{Y}_{\mathrm{LF}}}{\partial x_j} = \frac{\partial}{\partial x_j}\left(\bar{\rho}\left(\frac{\nu_T}{Sc_{\tilde{Y}_{\mathrm{LF}}}} + C_\rho\frac{k^2}{\epsilon}|\overline{Z''}|\right)\frac{\partial \tilde{Y}_{\mathrm{LF}}}{\partial x_j}\right) + \bar{w}_m \tag{16}$$

Total and LF variables are related according to the following relations:

$$\tilde{\varphi}|_{\mathrm{LF}} = \frac{\tilde{Z}/\tilde{Y}_{\mathrm{LF}} - Z_c}{1 - Z_c} \tag{17}$$

$$\tilde{R}_{\varphi}|_{\mathrm{LF}} = \frac{\tilde{R}_Z - \tilde{Y}_{\mathrm{LF}}(1-\tilde{Y}_{\mathrm{LF}})(\tilde{Z}/\tilde{Y}_{\mathrm{LF}})^2}{\tilde{Y}_{\mathrm{LF}}(1-Z_c)^2} \tag{18}$$

where $\tilde{R}_Z = \overline{\rho Z''^2}/\bar{\rho}$.

The equation for the total variance $\tilde{R}_Z$ is modified to take into account the mass-transfer rate. In particular, the mean scalar dissipation rate consists of two contributions:

1) The usual gaseous scalar dissipation is related to molecular diffusion effects.

2) A complementary contribution to dissipation incorporates the influence of the mass transfer between the HF and LF phases, because it also decreases the overall level of scalar fluctuations.

The following transport equation for the scalar-variance level can be derived (see the Appendix):

$$\begin{aligned}\frac{\partial \bar{\rho}\tilde{R}_Z}{\partial t} + \frac{\partial \bar{\rho}\tilde{u}_j\tilde{R}_Z}{\partial x_j} &= \frac{\partial}{\partial x_j}\left(\bar{\rho}\left(\frac{\nu_T}{Sc_{\tilde{Z}''^2}} + C_\rho\frac{k^2}{\epsilon}|\overline{Z''}|\right)\frac{\partial \tilde{R}_Z}{\partial x_j}\right)\\ &+ 2\bar{\rho}\left(\frac{\nu_T}{Sc_{\tilde{Z}}} + C_\rho\frac{k^2}{\epsilon}|\overline{Z''}|\right)\frac{\partial \tilde{Z}}{\partial x_j}\frac{\partial \tilde{Z}}{\partial x_j}\\ &- (1-Z_c)^2\underbrace{(C_\varphi\bar{\rho}\frac{\epsilon}{k}\tilde{Y}_{\mathrm{LF}}\tilde{R}_{\varphi}|_{\mathrm{LF}}}_{\text{standard dissipation}}\\ &+ \underbrace{(\tilde{R}_{\varphi}|_{\mathrm{LF}} - \tilde{\varphi}|_{\mathrm{LF}}(1-\tilde{\varphi}|_{\mathrm{LF}}))\frac{Z_c\bar{w}_m}{(1-Z_c)\tilde{\varphi}|_{\mathrm{LF}}})}_{\text{mass transfer dissipation}} - \bar{w}_m Z_c\end{aligned} \tag{19}$$

Note that the previous set of equations (16) and (19) is also valid for the more conventional situation of a two-phase flow of liquid and gas; the only difference is that in the present case, the mass-transfer term $\bar{w}_m$ describes the flux of gas that crosses the isosurface $Z = Z_c$ and not the classical vaporization process. The corresponding mass flux per unit area at the isosurface $Z = Z_c$ can be relatively small: HF and LF phases encounter difficulties mixing together, as evidenced by the presence of HDGM layers. A possible way to enhance the mass-transfer process is to increase the available surface of exchange through the breakup phenomena. This interface is increased by turbulent wrinkling and is decreased by molecular diffusion. At equilibrium (i.e., when these two competing processes balance each other), the mean surface density is sufficiently high to compensate the small interfacial flux in such a manner that the whole mass-transfer rate is finally driven by the turbulent mixing rate. In the first approximation, the mass-transfer term can be estimated by hypothesizing that the maximum value of gas mass fraction $\tilde{Y}_{\mathrm{LF}}^{\infty}$ in the LF mixture is reached with a characteristic time scale that is proportional to the integral turbulent time scale. The associated equilibrium value $(\bar{w}_v)^*$ corresponds to a turbulence-driven model for the mean mass-transfer rate, which can be expressed as follows:

$$(\bar{w}_m)^* = \bar{\rho}C_m\frac{\epsilon}{k}(\tilde{Y}_{\mathrm{LF}}^{\infty} - \tilde{Y}_{\mathrm{LF}}) \tag{20}$$

where $\tilde{Y}_{\mathrm{LF}}^{\infty}$ is given by

$$\begin{cases}\tilde{Y}_{\mathrm{LF}}^{\infty} = \tilde{Z}/Z_c & \text{if } \tilde{Z} < Z_c\\ \tilde{Y}_{\mathrm{LF}}^{\infty} = 1 & \text{if } \tilde{Z} > Z_c\end{cases} \tag{21}$$

In the absence of any further information concerning its value, the modeling constant C_m of Eq. (20) is set to unity. Another possibility that avoids the need to resort to such an algebraic closure for the mass-transfer rate $\bar{w}_m$ will be discussed in the next section.

The resulting model, called the LF-HF model, is applied to the Mascotte test case, and the result is displayed in Fig. 5. As expected, the flame length obtained with the modified turbulent flux model is smaller than before. The length and shape of the computed flame are very similar to the experimental flames. The flame expansion occurs slightly more upstream with the LF-HF than with the GG model. The obtained computational results seem to be in better agreement with then experimental data than those previously obtained up to now. Even if the experiments do not allow visualizing the whole flame area, the contraction that points out the end of the flame (clearly visible inside the measurement window) is well recovered with the LF-HF model, but not with the GG model.

Finally, the locations of the quantitative maxima of OH* emission and OH concentration, respectively, measured or estimated by each of the proposed models, are not in good agreement. Of course, the comparison is difficult because the two OH signals are quite different; in the experiments, only excited OH* emission is visible, whereas numerical simulations do not discriminate the excited from nonexcited OH radicals. Nevertheless, the maximum of OH* emission in the experiments is located near the injector, and this behavior is better recovered with the LF-HF model than with the GG model.

In the second step, to test the influence of the modeling-constant C_m, computations have been performed with three distinct values of this parameter. Corresponding results are reported in Fig. 6. The influence of this constant value is far from being straightforward, because two opposite effects are competing when increasing its value. On one hand, the characteristic time scale associated with the mass-transfer process is decreased by increasing C_m and this reduces the flame length. On the other hand, the density gradients are smoothed faster, and as a consequence, the magnitude of the turbulent liquid flux as given by the LF-HF model is decreased. Thus, the delay for HF dispersion increases: the flame is longer. Considering the results displayed in Fig. 6, the second effect seems to prevail, because as C_m is increased, the flame length increases. The shape of the flame also tends to be similar to that obtained with the GG model as C_m increases. Considering the available experimental results, the value $C_m = 1.0$ leads to the best agreement with experiments, and this value is retained in the subsequent steps of the analysis.

In Fig. 7, the mean density fields obtained with the LF-HF model are also reported for increasing values of the modeling constant C_m. In the same figure, the result obtained with the GG model is also given as a reference at the bottom. The drastic influence of the present closure assumption is clearly put into evidence: the liquid-core length is strongly reduced by the use of the modified model for the turbulent liquid flux. As the constant value C_m is increased, the

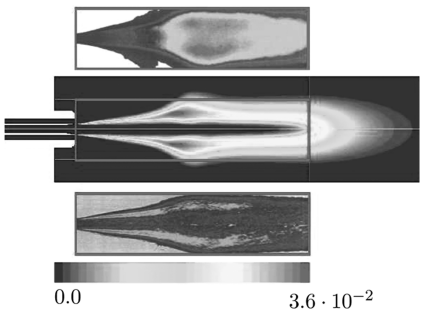

Fig. 5 Computed fields of OH mass fraction for the LF-HF model; constant C_m is set to unity; average measured OH* emission field (top) and Abel inverted image (bottom).

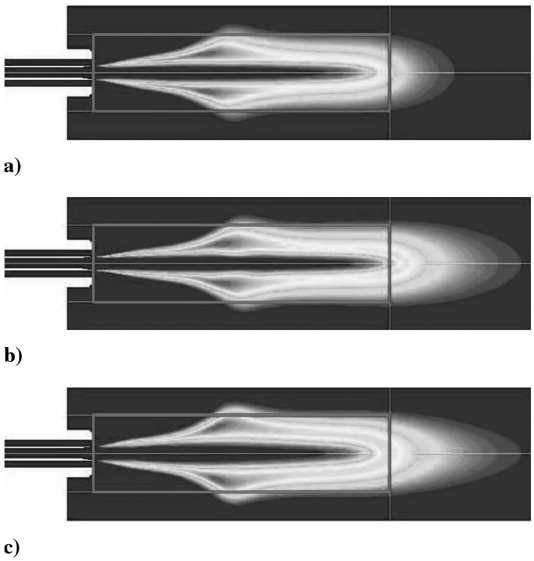

Fig. 6 Computed fields of OH mass fraction obtained with the LF-HF model: a) $C_m = 0.5$ ($Y_{OH}^{\max} = 0.0314$), b) $C_m = 1.0$ ($Y_{OH}^{\max} = 0.0354$), and c) $C_m = 2.0$ ($Y_{OH}^{\max} = 0.0429$).

behavior of the LF-HF model is expected to recover the one obtained with the GG model, but this limit can be reached only for very large values of the modeling constant C_m. The latter situation corresponds to an infinitely fast mass-transfer rate.

The remarkable influence of the model used to represent the turbulent flux on the density field is evidenced in Fig. 7, which compares LF-HF results to GG results. In [8], the ability of different approaches [RANS, unsteady RANS (URANS), and LES] to represent GO2-GH2 supercritical combustion has been evaluated. It is interesting to take a closer look at the results presented in Figs. 6e and 6f of [8]: for the unsteady simulations (LES and URANS), the obtained lengths of the preserved core, in which O2 concentration

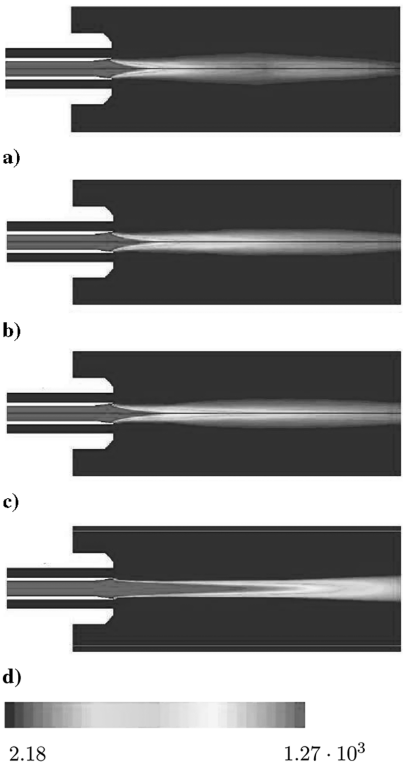

Fig. 7 Computed fields of mean density for the a) LF-HF model with $C_m = 0.5$, b) LF-HF model with $C_m = 1.0$, c) LF-HF model with $C_m = 2.0$, and d) GG model.

values are close to unity, are found to be very short in comparison with that obtained with the RANS computation. In the corresponding RANS simulation, the model proposed here for the turbulent flux (i.e., the LF-HF model) is not applied, and without the correction we proposed, it seems that the length of the dense zone can be greatly overestimated. This is in complete agreement with both the present results and our previous analysis of [5], and it may be concluded that RANS models can satisfactorily describe supercritical turbulent mixing, provided that a special modeling is retained to describe the turbulent scalar flux.

VII. LF-HF Model Supplemented by a Mean Surface-Density Equation: The LF-HF-Σ Model

In the previous section, the mass-transfer rate was evaluated by assuming that an equilibrium is reached between the production of Z_c isosurface by turbulent straining and its dissipation due to molecular diffusion effects. However, reaching such an equilibrium requires a finite delay. Such a delay can be taken into account through a modeled transport equation for this quantity. The derivation and closure of such a transport equation has been the subject of many earlier studies since the first step made in this direction by Marble and Broadwell [42]. Further developments have been done in the field of turbulent combustion by Candel and Poinsot [43]. More recently, a similar transport equation for the mean surface density of liquid has been considered in [14,17] to describe the atomization processes, and Jay et al. [2] also proposed a special closure of the equation devoted to coaxial injection under supercritical conditions. In the present study, we use the general transport equation for the surface density proposed in [14,17,20]. The corresponding modeled transport equation takes the following form:

$$\frac{\partial \Sigma}{\partial t} + \frac{\partial \tilde{u}_j \Sigma}{\partial x_j} = \frac{\partial}{\partial x_j}\left(\frac{\nu_T}{\mathrm{Sc}_\Sigma} + C_\rho \frac{k^2}{\epsilon}|\overline{Z''}|\right)\frac{\partial \Sigma}{\partial x_j} + 2\left(\frac{\nu_T}{\mathrm{Sc}_{\tilde{Y}_{\mathrm{HF}}}} + C_\rho \frac{k^2}{\epsilon}|\overline{Z''}|\right)\frac{1}{l_T}\frac{\partial \bar{\Phi}_{\mathrm{HF}}}{\partial x_j}\frac{\partial \bar{\Phi}_{\mathrm{HF}}}{\partial x_j} + C_\Sigma \frac{\epsilon}{k}\left(\Sigma - \frac{\Sigma^2}{\Sigma_c}\right) \tag{22}$$

where $\bar{\Phi}_{\mathrm{HF}}$ is the mean volume fraction of heavy fluid $\bar{\Phi}_{\mathrm{HF}} = \bar{\rho}\tilde{Y}_{\mathrm{HF}}/\rho_{\mathrm{HF}}$, and Sc_Σ and $Sc_{\tilde{Y}_{\mathrm{HF}}}$ are two turbulent Schmidt numbers set to 0.7. The main difference between the present equation and that used in [14,17] lies in the turbulent transport terms modeled by using the modified turbulent diffusion law of Eq. (9).

Concerning the production–destruction terms, the strain rate due to turbulent fluctuations is estimated from the integral characteristic time scale $\tau_T = k/\epsilon$. Finally, the surface-density growth by turbulence is bounded by a consumption term proportional to Σ^2. Also note that a critical value Σ_c has been introduced in Eq. (22).

This general form of the Σ equation must be now modified to describe supercritical thermophysical conditions. The first modification concerns the critical value Σ_c. In usual two-phase flows of liquid and gas, this value has been related to a critical value of the Weber number, as described in [14,17]. In this case, the maximum value of Σ is directly connected to the equilibrium state, which is reached as soon as the surface-tension effect is able to prevent any further breakup or liquid fragmentation. In supercritical conditions, the situation is quite different, because an equilibrium is expected between production by turbulent straining and destruction by molecular diffusion at the interface $Z = Z_c$ (i.e., the mass-transfer process).

In fact, in supercritical conditions, surface tension does not come into play. Note that the surface under consideration corresponds to the HDGM layers that separate the HF from the LF. Hence, the minimum expected size for the HF pockets as they are defined in the LF-HF model must be related to the molecular diffusion processes that take place at $Z = Z_c$. Indeed, the surface density Σ increases under the influence of turbulent wrinkling processes, and this means that smaller and smaller HF structures are produced. Once they are small enough, they are dissipated through molecular diffusion, and

the characteristic length scale of the corresponding small-scale structures is related to the Batchelor scale:

$$\eta_B = \eta_K Sc^{1/2} \tag{23}$$

where $\eta_K = (\nu^3/\epsilon)^{1/4}$ is the Kolmogorov length scale, and $Sc = \nu/D$ is the molecular Schmidt number.

Now the critical value Σ_c must be related to the Batchelor scale. The presence of the HDGM surface requires the simultaneous presence of HF and LF. The probability of presence of the HF phase can be estimated by the mean volume fraction of HF, denoted by $\bar{\Phi}_{\mathrm{HF}}$. In the same way, the probability of presence of the LF phase can be obtained through the LF mean volume fraction $\bar{\Phi}_{\mathrm{LF}}$. As a result, a measure of the probability of the HDGM surface is given by the product $\bar{\Phi}_{\mathrm{LF}}\bar{\Phi}_{\mathrm{HF}}$. Moreover, the mean density of surface is dependent on the characteristic length scales of both components: the smaller the characteristic length scale, the higher the surface density. Finally, the following expression is retained to evaluate the critical value of the mean surface density:

$$\Sigma_c = \frac{\bar{\Phi}_{\mathrm{LF}}\bar{\Phi}_{\mathrm{HF}}}{\eta_B} \tag{24}$$

With the modeled surface-density equation now established, the next step is to estimate the mass-transfer rate in Eq. (19), taking the surface growth into account. Here, the essential hypothesis is that even under supercritical conditions, the flux of LF per unit surface at $Z = Z_c$ (the particular isosurface that defines the boundary between HF and LF) is smaller than for any other value of Z in the LF phase. This assumption corresponds to the hypothesis already proposed in [11] and is introduced to mimic the expected phenomenology that the lifetime of a fluid pocket is dependent on its density. Hence, the local mass-transfer rate per unit surface W_m is expected to be small, but the total mass-transfer rate $\bar{w}_m = W_m\Sigma$ can increase as the available mean surface density Σ increases. The mass-transfer rate per unit surface W_m depends on the local conditions at the surface, such as the density gradient and the molecular diffusion coefficient.

However, the total mass-transfer rate can become independent of these local conditions at the surface that separates HF and LF phases. Indeed, the corresponding surface density increases to reach the limit Σ_c, and this limit is reached when the product $\bar{w}_m = W_m\Sigma$ becomes independent of the local conditions at the surface. When this limiting state is reached, the total mass-transfer rate $\bar{w}_m$ tends toward the previously defined mass-transfer rate $(\bar{w}_v)^*$ of Eq. (20) and becomes driven by the turbulent mixing processes only.

This phenomenological description is similar to the high-Reynolds-number turbulence representation in which the fragmentation or cascade process makes the turbulent dissipation rate independent of molecular viscosity. In this special case, the velocity gradients at small scales exactly compensate the molecular viscous effects that dissipate the turbulent kinetic energy produced at large scales. Conversely, in the present case, the surface density grows until it reaches a sufficient level, with respect to the molecular diffusion effects, to ensure the mixing of the total flux of injected heavy fluid. This is why the final total mass-transfer rate $\bar{w}_m$ must be independent of the local molecular diffusion coefficient. The role of the molecular diffusion is to fix the time needed to reach this final state: the smaller the molecular diffusion flux, the more important the surface density to be created. Taking this phenomenology into account, the total mass-transfer rate is approximated through the following linear relationship:

$$\bar{w}_m = \frac{\Sigma}{\Sigma_c}(\bar{w}_m)^* \tag{25}$$

implying that the identity $\bar{w}_v = (\bar{w}_m)^*$ is recovered at the equilibrium state (i.e., when $\Sigma = \Sigma_c$).

Figure 8 displays the computational OH concentration obtained with the LF-HF-Σ model. It is compared with the measurement of the excited OH*, and the best agreement is again obtained with a modeling-constant C_m value set to unity. In Fig. 9, the field of mean surface density Σ obtained with the LF-HF-Σ model is reported. The obtained results do not appear to be strongly influenced by the mass-transfer-rate modeling through the use of a modeled transport equation for the mean surface density, and the previous infinitely fast mass-transfer closure proposal, as given by Eq. (20), gave just as satisfactory results. This specific feature is in accordance with the experimental analysis conducted by Juniper et al. [37], who concluded that vaporization and turbulent mixing processes exchange their dominating influence on the combustion rate from low pressures, in which vaporization is the driving phenomena, to high pressures, in which the turbulent mixing becomes the key parameter. It seems that for the high-pressure conditions considered in the present study, the detailed modeling of the mass-transfer rate does not play a critical role.

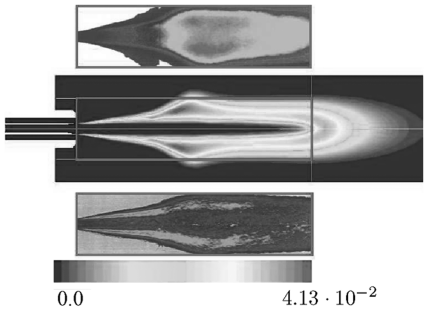

Fig. 8 Computed fields of OH mass fraction obtained with the LF-HF-Σ equation. Average measured OH* emission field (top) and Abel inverted image (bottom).

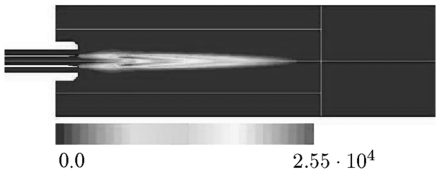

Fig. 9 Computed field of the surface density Σ obtained with the LF-HF-Σ.

Finally, the reported comparisons with available experimental data show that the results of the present numerical simulations are more sensitive to the modeling of the large-density-variation effects (represented through the LF-HF model) than to the mass-transfer rate description through the modeled Σ transport equation.

VIII. Application to a Lower Momentum Flux Ratio

In the last section of the paper, the present modeling proposals (namely, GG, LF-HF, and LF-HF-Σ) are applied to the second available experimental test case, which corresponds to a momentum flux ratio $J \approx 6$. Compared with the previous test case, the momentum flux ratio value J is 2 times smaller than before. The middle picture of Fig. 10 shows the experimental Abel inverted average image as obtained by Juniper et al. [37]. As previously stressed in [37], the comparison with Fig. 8 shows that with the present value of J the hydrogen excess is less important and the flame extends to a larger radius after 12 diameters downstream of the injector exit.

The result obtained with the GG model is reported at the top of Fig. 10 and the result obtained with the LF-HF model is displayed at the bottom. The LF-HF model is able to predict the evolution of the OH concentration radical, with the maxima located nearly parallel to the symmetry axis, as observed in the experiments performed in the second downstream part of the flame. In contrast, the GG model predicts a divergence of these lines associated with the location of OH emission maxima. Moreover, the bump observed between 3 and 4 diameters downstream of the injector exit is recovered with the LF-HF model but not with the GG model.

Finally, Fig. 11 displays the results obtained with the LF-HF model either with or without the modeled transport equation for the

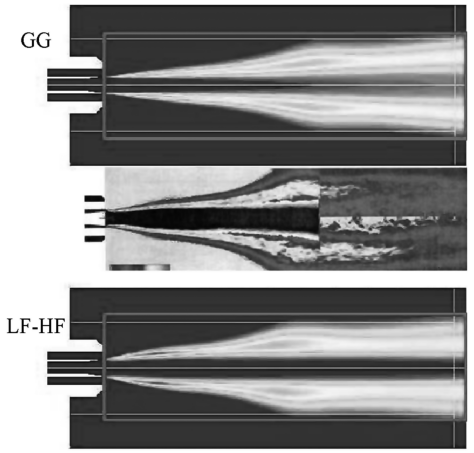

Fig. 10 Result obtained with the GG model (top) and with the LF-HF model (bottom); $C_m = 1$; test case with a momentum flux ratio $J \approx 6$ [27].

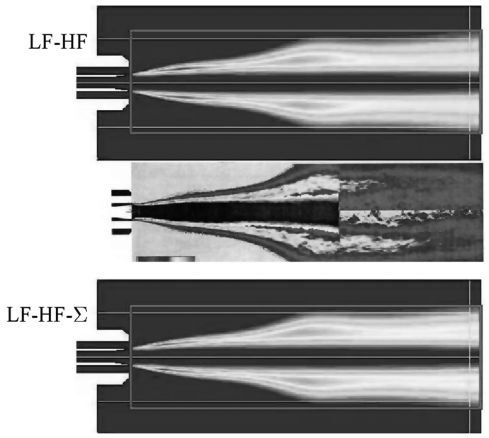

Fig. 11 Results obtained with LF-HF models: LF-HF model (top) and LF-HF-Σ model (bottom); test case with a momentum flux ratio $J \approx 6$ [27].

mean surface density Σ. The obtained results are both qualitatively correct. The behaviors of the two models are very similar and it is quite difficult to discriminate one with respect to the other, at least with the available experimental data, which emphasizes that additional experimental investigations are necessary to complement this test case to perform a complete validation of the predictivity of the different models proposed in this work.

Finally, it should be remembered that the model relies on the fast-chemistry hypothesis, a feature that can become inappropriate under certain circumstances, but it has the potentiality to be extended, without major difficulties, to the consideration of finite rate chemistry effects by using, for instance, the methodology proposed in [44].

IX. Conclusions

In the search of a satisfactory closure for turbulent combustion in supercritical conditions, a hierarchy of three original RANS models has been proposed and tested in conditions representative of cryogenic rocket engines. The three modeling proposals rely on the infinitely-fast-chemistry hypothesis, and the classical Beta function is used to presume the mixture-fraction PDF shape. Each closure gradually includes an additional feature that is relevant for the supercritical turbulent reactive flows under consideration:

1) The first closure is very classical and relies on a tabulated chemistry approach that incorporates the real-gas effects on the density of the oxygen as obtained from a Benedict–Webb–Rubin equation of state. The corresponding closure is denoted as the GG model.

2) Concerning the influence of the large density fluctuations, which seems to be the predominant effect in the present conditions, the second and third closures rely on a previous modeling proposal originally introduced to describe liquid dispersion in two-phase flows from an Eulerian point of view. The important role of a new variable associated with the level of density difference is established. The model is extended to describe the turbulent mixing between liquid oxygen (LOx) and gaseous hydrogen (GH2) in supercritical conditions:

a) A new presumed PDF shape is introduced.

b) Additional source terms are considered in the transport equation of the mixture-fraction variance.

c) A specific closure for the supercritical mass-transfer rate is put forward and incorporated. The resulting approach is denoted as LH-HF.

3) Finally, the third model generalizes the second proposal and includes a mean transport equation for the density of the surface that separates the HF from the LF. The resulting model LF-HF-Σ is expected to provide better results by improving the description of the mass-transfer rate between the two phases: a key quantity from the turbulent combustion modeling point of view, especially within the infinitely-fast-chemistry limit.

The three models are applied to an experimental test case consisting of a low-speed round jet of LOx atomized by an high-speed annular GH2 coflowing jet under supercritical conditions. Despite the complexity of the corresponding turbulent reactive flow, the numerical results obtained with the simplest approach (i.e., the GG model) are able to recover the essential trends given by the experimental results. Nevertheless, the lengths of the nonpremixed flame are overestimated and the predictions are significantly improved when the LF-HF model is used. In the LF-HF approach, by analogy with a two-phase flow of liquid and gas, the dense and the light components are considered separately. This approach is specifically developed to deal with the huge density variations that exist in supercritical combustion. Such density variations, from 6 kg/m^3 in the GH2 stream to 6 kg/m^3 in the LOx stream, are not encountered in usual conditions. The latter modeling proposal allows a fairly good recovery of the experimental results for two distinct cases featuring very different values of the momentum flux ratio between hydrogen and oxygen streams.

To the knowledge of the present authors, the agreement between the results presented here and the experimental data obtained for this well-known test case seems better than even reported before. The LF-HF model also provides a good estimate of penetration lengths of the dense stream. From this point of view, the LF-HF model gives results in accordance with other published results obtained through LES computations. In the LF-HF model, the mass-transfer rate between the dense and the light streams is introduced in an attempt to evaluate the net flux of LOx at the surface that separates HF and LF phases.

In the second step of the present analysis, the mass-transfer rate is described through an equation for the mean surface density that is able to take into account the specific features of the small-scale dynamics of supercritical flows. In supercritical flows, this surface does not correspond to a thermodynamic one (i.e., the interface that separates liquid from gas), but to the HDGM layers that have been already observed in DNS studies. Nevertheless, the consideration of a mean surface-density transport equation does not give rise to significant improvements of the computational results with respect to the available experimental data. This is in accordance with recent experimental investigations that have evidenced the turbulent mixing process as the leading mechanism at elevated pressures.

Finally, the main conclusion that can drawn from the present study devoted to turbulent mixing and combustion in supercritical conditions is twofold:

1) The performed analysis confirms that the description of turbulent transport in supercritical conditions requires special care within the RANS approach. The results of numerical simulations can be significantly improved by considering a closure that includes the influence of the large density ratio that exists between the LOx and GH2 streams.

2) In contrast, concerning the small-scale mass-transfer rate, the use of a very simple closure based on the turbulent strain rate ϵ/k is

sufficient to recover the essential trends that are observed in the experimental database.

Appendix: Derivation of a Modeled Transport Equation for the Mixture-Fraction Variance

Evolution of the variance field of the total mixture fraction Z is described through Eq. (12), and this exact but unclosed equation requires additional closure assumptions. In particular, the terms that involve the turbulent flux of the mean $\tilde{Z}$ and the variance $\tilde{R}_Z = \overline{\rho Z''^2}/\bar{\rho}$ are represented by the modified turbulent-dispersion model

$$-\overline{\rho u_j'' R_Z} = -\overline{\rho u_j'' Z''^2} = \bar{\rho}\left(\frac{\nu_T}{Sc_{\tilde{Z}''^2}} + C_\rho \frac{k^2}{\epsilon}|\overline{Z''}|\right)\frac{\partial \tilde{R}_Z}{\partial x_j} \tag{A1}$$

and

$$-\overline{\rho u_j'' Z''} = \bar{\rho}\left(\frac{\nu_T}{Sc_{\tilde{Z}}} + C_\rho \frac{k^2}{\epsilon}|\overline{Z''}|\right)\frac{\partial \tilde{Z}}{\partial x_j} \tag{A2}$$

and only the scalar dissipation term still remains to be closed. The simplest and most widely used representation for this term is the linear relaxation model:

$$\epsilon_Z = C_Z \frac{\epsilon}{k}\tilde{R}_Z \tag{A3}$$

Here, it is proposed to extend this closure to account for both 1) vaporization (in supercritical conditions, this is the mass transfer between the LF and HF phases), and 2) mixing between the two components.

As discussed in Sec. VI, the LF phase is described through the first two moments of the variable φ: namely, $\tilde{\varphi}|_{\mathrm{LF}}$ and $\tilde{R}_\varphi|_{\mathrm{LF}} = \overline{\rho\varphi''^2}/\bar{\rho}$. The correspondence between HF and LF variables is given by Eq. (17).

Because the LF mixture is supposed to be described by standard laws, the PDF shape is assumed to be a classical β function with a scalar dissipation term as given by the linear relaxation model for scalar fluctuations. Nevertheless, to take into account the influence of the mass-transfer process, additional modifications should be brought to the modeling.

Indeed, as the mass-transfer rate from HF to LF is mainly driven by the mixing processes at the vicinity of the HDGM surface, every particle that issued from the HF phase keeps pace with a small amount of LF, and the turbulent mixing and mass-transfer processes appear to be strongly correlated. To get an insight into the modifications that are likely to appear in the corresponding scalar transport equations, the two processes are first considered in the simpler case of a turbulent homogeneous flow with a constant mean scalar value $\tilde{Z}$.

In this special case, the mixture-fraction PDF $\tilde{P}(Z)$ evolves only under the action of vaporization (or mass transfer in supercritical conditions) and micromixing in the composition space. Moreover, because all of the mean gradient terms vanish, the evolution of the total variance level is driven by scalar dissipation:

$$\frac{d\tilde{R}_Z}{dt} = -\epsilon_Z \tag{A4}$$

Keeping in mind that $\tilde{R}_Z$ and $\tilde{R}_\varphi|_{\mathrm{LF}}$ are interrelated through

$$\tilde{R}_Z = (\tilde{R}_\varphi|_{\mathrm{LF}} - \tilde{\varphi}|_{\mathrm{LF}}(1-\tilde{\varphi}|_{\mathrm{LF}}))\tilde{Y}_{\mathrm{LF}}(1-Z_c)^2 + \tilde{Z}(1-\tilde{Z}) + Z_c(\tilde{Z}-\tilde{Y}_{\mathrm{LF}}) \tag{A5}$$

and differentiating this equation with respect to time yields the following expression for the total scalar dissipation rate:

$$-\epsilon_Z = (1-Z_c)^2((\tilde{R}_\varphi|_{\mathrm{LF}} - \tilde{\varphi}|_{\mathrm{LF}}(1-\tilde{\varphi}|_{\mathrm{LF}}))\frac{\bar{w}_m}{\bar{\rho}} + \tilde{Y}_{\mathrm{LF}}\frac{d}{dt}(\tilde{R}_\varphi|_{\mathrm{LF}} - \tilde{\varphi}|_{\mathrm{LF}}(1-\tilde{\varphi}|_{\mathrm{LF}}))) - \frac{Z_c\bar{w}_m}{\bar{\rho}} \tag{A6}$$

Moreover, the following relation holds between the total averaged mixture fraction $\tilde{Z}$ and its LF counterpart $\tilde{\varphi}|_{\mathrm{LF}}$:

$$\tilde{Z} = (1-Z_c)(\tilde{\varphi}|_{\mathrm{LF}}) + Z_c \tag{A7}$$

The definition of the mean value together with the scalar PDF expression given by Eq. (15) leads to

$$\frac{d\tilde{Z}}{dt} = \frac{d}{dt}\int_0^1 Z\tilde{Y}_{\mathrm{HF}}\delta(Z)\mathrm{d}Z + \frac{d}{dt}\int_0^1 Z\frac{\tilde{Y}_{\mathrm{LF}}}{1-Z_c}\tilde{P}_\varphi(\varphi)\mathrm{d}Z \tag{A8}$$

$$\frac{d\tilde{Z}}{dt} = \frac{d\tilde{Y}_{\mathrm{LF}}}{dt}(\tilde{\varphi}|_{\mathrm{LF}}(1-Z_c)+Z_c) + \tilde{Y}_{\mathrm{LF}}\frac{d}{dt}(\tilde{\varphi}|_{\mathrm{LF}}(1-Z_c)+Z_c) \tag{A9}$$

Because $\tilde{Z}$ is constant in homogeneous conditions and because the variation of $\tilde{Y}_{\mathrm{LF}}$ is directly given by the mass-transfer rate $\bar{w}_m/\bar{\rho}$, the evolution of $\tilde{\varphi}|_{\mathrm{LF}}$ writes as

$$\frac{d\tilde{\varphi}|_{\mathrm{LF}}}{dt} = -\frac{\bar{w}_m}{\bar{\rho}\tilde{Y}_{\mathrm{LF}}}\left(\tilde{\varphi}|_{\mathrm{LF}} + \frac{Z_c}{1-Z_c}\right) \tag{A10}$$

Unfortunately, the variation of $\tilde{R}_\varphi|_{\mathrm{LF}}$ cannot be obtained in such a straightforward manner. The problem is to evaluate to what extent the PDF of φ is influenced by the mass-transfer processes. It can be argued that particles with a value of φ close to zero are probably more sensitive to this influence than the others, but in the absence of any further quantitative information, the most general procedure consists of considering that all particles are affected by the mass transfer with the same probability, whatever their value φ.

Starting from a β function PDF of φ defined through its mean value $\tilde{\varphi}|_{\mathrm{LF}}$ and variance $\tilde{R}_\varphi|_{\mathrm{LF}}$, in the first step of the analysis, we can consider that no micromixing takes place in the LF phase (i.e., $\epsilon_\varphi = 0$). In this special case, the PDF of φ denoted by $\tilde{P}^*(\varphi)$ is given by the initial β PDF plus a Dirac delta peak at $\varphi = 0$ that results from the mass transfer from the HF phase to the LF phase:

$$\tilde{P}^*(\varphi) = \alpha\beta(\tilde{\varphi}|_{\mathrm{LF}}, \tilde{R}_\varphi|_{\mathrm{LF}}) + (1-\alpha)\delta(\varphi) \tag{A11}$$

This PDF shapes leads to $\tilde{\varphi}|^*_{\mathrm{LF}} = \alpha\tilde{\varphi}|_{\mathrm{LF}}$ and $\widetilde{\varphi^2}|^*_{\mathrm{LF}} = \alpha\widetilde{\varphi^2}|_{\mathrm{LF}}$. Equation (A10) is still valid for $\tilde{\varphi}|^*_{\mathrm{LF}}$; therefore,

$$\frac{d\alpha}{dt} = \frac{\bar{w}_m}{\bar{\rho}\,\tilde{\varphi}\,|_{\mathrm{LF}}\tilde{Y}_{\mathrm{LF}}}\left(\tilde{\varphi}|^*_{\mathrm{LF}} + \frac{Z_c}{1-Z_c}\right) \tag{A12}$$

Thus,

$$\frac{d\widetilde{\varphi^2}|^*_{\mathrm{LF}}}{dt} = \frac{\bar{w}_m}{\bar{\rho}\,\tilde{\varphi}\,|_{\mathrm{LF}}\tilde{Y}_{\mathrm{LF}}}\left(\tilde{\varphi}|^*_{\mathrm{LF}} + \frac{Z_c}{1-Z_c}\right)\widetilde{\varphi^2}|_{\mathrm{LF}} \tag{A13}$$

In the second step, micromixing is now taken into account (i.e., $\epsilon_\varphi \neq 0$). In this case, no Dirac delta peak at $\varphi = 0$ will be maintained, because any particle that issued from the HF phase is redistributed in the φ composition space, due to the micromixing effects. To express this phenomenon, the scalar dissipation is considered on the whole PDF with the standard linear model:

$$\epsilon_\varphi = C_\varphi \frac{\epsilon}{k}\tilde{R}_\varphi|_{\mathrm{LF}} \tag{A14}$$

The contributions of both mass transfer and micromixing are then considered and we assume that the β-shaped PDF is still valid to represent scalar fluctuations. Finally, one can note that

$$\tilde{R}_\varphi|_{\mathrm{LF}} - \tilde{\varphi}|_{\mathrm{LF}}(1-\tilde{\varphi}|_{\mathrm{LF}}) = \widetilde{\varphi^2}|_{\mathrm{LF}} - \tilde{\varphi}|_{\mathrm{LF}}$$

which gives

$$\frac{d}{dt}(\tilde{R}_\varphi|_{\mathrm{LF}} - \tilde{\varphi}|_{\mathrm{LF}}(1-\tilde{\varphi}|_{\mathrm{LF}})) = \frac{\bar{w}_m}{\bar{\rho}\tilde{Y}_{\mathrm{LF}}}\left(1 + \frac{Z_c}{\tilde{\varphi}|_{\mathrm{LF}}(1-Z_c)}\right) \times (\tilde{R}_\varphi|_{\mathrm{LF}} - \tilde{\varphi}|_{\mathrm{LF}}(1-\tilde{\varphi}|_{\mathrm{LF}})) - C_\varphi \frac{\epsilon}{k}\tilde{R}_\varphi|_{\mathrm{LF}} \quad \text{(A15)}$$

The last expression is used in Eq. (A6) to recover the final expression for the total scalar dissipation as given by Eq. (19):

$$-\bar{\rho}\epsilon_Z = -(1-Z_c)^2\left(C_\varphi\bar{\rho}\frac{\epsilon}{k}\tilde{Y}_{\mathrm{LF}}\tilde{R}_\varphi|_{\mathrm{LF}} + (\tilde{R}_\varphi|_{\mathrm{LF}} - \tilde{\varphi}|_{\mathrm{LF}}(1-\tilde{\varphi}|_{\mathrm{LF}}))\frac{Z_c\bar{w}_m}{(1-Z_c)\tilde{\varphi}|_{\mathrm{LF}}}\right) - \bar{w}_m Z_c \quad \text{(A16)}$$

Acknowledgments

The authors would like to acknowledge the financial support from Centre National de la Recherche Scientifique, Centre National d'Etudes Spatiales, and Société Nationale d'Etude et de Construction de Moteurs d'Aviation, Space Engine Division (SAFRAN Group). They also wish to thank Roland Borghi (Laboratoire de Mécanique et d'Acoustique, Marseille, France) and Michel Champion (Laboratoire de Combustion et de Détonique, Poitiers, France) for interesting discussions concerning this work.

References

[1] Haidn, O., and Habiballah, M., "Research on High Pressure Cryogenic Combustion," *Aerospace Science and Technology*, Vol. 7, No. 6, 2003, pp. 473–491. doi:10.1016/S1270-9638(03)00052-X

[2] Jay, S., Lacas, F., and Candel, S. M., "Combined Surface Density Concepts for Dense Spray Combustion," *Combustion and Flame*, Vol. 144, No. 3, 2006, pp. 558–577. doi:10.1016/j.combustflame.2005.07.017

[3] Borghi, R., and Burluka, A. A., "Simple Model for Turbulent Two-Phase Combustion with Fast Chemistry," *ZAMM*, Vol. 79, 1999, pp. 537–540.

[4] Borghi, R., and Burluka, A. A., "Vers une Nouvelle Modélisation des Flammes Diphasiques LOx-Hydrogène," *Combustion*, Vol. 2, No. 1, 2003, pp. 1–23.

[5] Demoulin, F. X., Beau, P. A., Blokkeel, G., Mura, A., and Borghi, R., "A New Model for Turbulent Flows With Large Density Fluctuations: Application to Liquid Atomization," *Atomization and Sprays*, Vol. 17, No. 4, 2007, pp. 315–345. doi:10.1615/AtomizSpr.v17.i4.20

[6] Oefelein, J. C., "Thermophysical Characteristics of LOx-H2 Flames at Supercritical Pressure," *Proceedings of the Combustion Institute*, Vol. 30, 2005, pp. 2929–2937. doi:10.1016/j.proci.2004.08.212

[7] Oefelein, J. C., "Mixing and Combustion of Cryogenic Oxygen-Hydrogen Shear-Coaxial Jet Flames at Supercritical Pressures," *Combustion Science and Technology*, Vol. 178, Nos. 1–3, 2006, pp. 229–252. doi:10.1080/00102200500325322

[8] Tucker, P. K., Menon, S., Merkle, C. L., Oefelein, J. C., and Yang, V., "An Approach to Improve Credibility of CFD Simulations for Rocket Injector Design," 43rd AIAA/ASME/SAE/ASEE Joint Propulsion Conference, AIAA Paper 2007-5572, July 2007.

[9] Yang, V., "Modeling of Supercritical Vaporization, Mixing, and Combustion Processes in Liquid-Fueled Propulsion Systems," *Proceedings of the Combustion Institute*, Vol. 28, 2000, pp. 925–942.

[10] Miller, R. S., Harstad, K. G., and Bellan, J., "Direct Numerical Simulations of Supercritical Fluid Mixing Layers Applied to Heptane-Nitrogen," *Journal of Fluid Mechanics*, Vol. 436, 2001, pp. 1–39.

[11] Okong'o, N. A., and Bellan, J., "Direct Numerical Simulation of a Transitional Supercritical Binary Mixing Layer: Heptane and Nitrogen," *Journal of Fluid Mechanics*, Vol. 464, 2002, pp. 1–34.

[12] Okong'o, N. A., Harstad, K., and Bellan, J., "Direct Numerical Simulations of O2/H2 Temporal Mixing Layers Under Supercritical Conditions," *AIAA Journal*, Vol. 40, No. 5, 2002, pp. 914–926. doi:10.2514/2.1728

[13] Okong'o, N. A., and Bellan, J., "Turbulence and Fluid-Front Area Production in Binary-Species, Supercritical, Transitional Mixing Layers," *Physics of Fluids*, Vol. 16, No. 5, 2004, pp. 1467–1492. doi:10.1063/1.1688326

[14] Vallet, A., Burluka, A. A., and Borghi, R., "Development of an Eulerian model for the Atomization of a Liquid Jet," *Atomization and Sprays*, Vol. 11, No. 6, 2001, pp. 619–642.

[15] Lebas, R., Blokkeel, G., and Demoulin, F. X., "Coupling Vaporization Model with the Eulerian-Lagrangian Spray Atomization (ELSA) Model in Diesel Engine Conditions," Society of Automotive Engineers TP 2005-01-0213, Apr. 2005.

[16] Okong'o, N. A., and Bellan, J., "A Priori Analysis of Subgrid-Scale Models for Large Eddy Simulations of Supercritical Binary-Species Mixing Layers," AIAA Paper 2005-155, Jan. 2005.

[17] Vallet, A., and Borghi, R., "Modélisation Eulérienne de l'Atomisation d'un Jet Liquide," *Comptes Rendus à l'Académie des Sciences*, Série IIb, Vol. 327, 1999, pp. 1015–1020. doi:10.1016/S1287-4620(00)87013-1

[18] Blokkeel, G., Mura, A., Demoulin, F. X., and Borghi, R., "A Continuous Modelling Approach for Describing the Atomization Process from Inside the Injector to the Final Spray," *Proceedings of the Ninth International Conference on Liquid Atomization and Spray Systems (ICLASS)* [online proceedings], July 2003, http://www.ilass.-soton.ac.uk/europe/procs.htm.

[19] Blokkeel, G., Demoulin, F. X., and Borghi, R., "Modelling of Two-Phase Flows: An Eulerian Model for Diesel Injection," *Thermo and Fluid Dynamics Processes in Diesel Engines*, edited by J. H. Whitelaw, F. Payri, C. Arcoumanis, J. M. Desantes, Springer–Verlag, Berlin, Vol. 2, 2004, pp. 87–105.

[20] Beau, P. A., and Demoulin, F. X., "A Multiphase Flow Approach and a Single-Phase Flow Approach in the Context of a Euler Model for Primary Breakup," *Proceedings of ILASS (Europe)* [online proceedings], Sept. 2004, http://www.ilass.soton.ac.uk/europe/procs.htm.

[21] Drew, D. A., "Mathematical Modeling of Two-Phase Flows," *Annual Review of Fluid Mechanics*, Vol. 15, 1983, pp. 261–291. doi:10.1146/annurev.fl.15.010183.001401

[22] Carreau, J. L., Le Visage, D., Monote, G., Gicquel, P., and Roger, F., "Characterization of the Near-Injector Region of Coaxial Jets," *Proceedings of the Sixth International Conference on Liquid Atomization and Spray Systems (ICLASS)* [online proceedings], July 1994 http://www.ilass.soton.ac.uk/europe/procs.htm.

[23] Stepowski, D. A., and Werquin, O., "Measurement of the Liquid Volume Fraction and Its Statistical Distribution in the Near Development of a Spray," *Atomization and Sprays*, Vol. 14, No. 3, 2004, pp. 243–264. doi:10.1615/AtomizSpr.v14.i3.30

[24] Lasheras, J. C., Villermaux, E., and Hopfinger, E. J., "Breakup and Atomization of a Round Water Jet by a High-Speed Annular Air Jet," *Journal of Fluid Mechanics*, Vol. 357, 1998, pp. 351–379. doi:10.1017/S0022112097008070

[25] Villermaux, E., Marmottant, P., and Duplat, J., "Ligament-Mediated Spray Formation," *Physical Review Letters*, Vol. 92, No. 7, 2004, pp. 074501.1–074501.4.

[26] Marmottant, P., and Villermaux, E., "On Spray Formation," *Journal of Fluid Mechanics*, Vol. 498, 2004, pp. 73–111. doi:10.1017/S0022112003006529

[27] Nicole A., Vingert L., and Habiballah, M., "Test Case RCM-2, Mascotte Single Injector 60 Bar," *Proceedings of the 3rd International Workshop on Rocket Combustion Modeling*, edited by S. Zurbach, Mar. 2006.

[28] Younglove, B. A., "Thermophysical Properties of Fluids. Part 1: Argon, Ethylene, Parahydrogen, Nitrogen, Nitrogen Trifluoride, Oxygen," *Journal of Physical Chemistry*, Vol. 11, sup. 1, 1982, pp. 1–368.

[29] Press, W. H., Flannery, B. P., Teukolsky, S. A., and Vetterling, W. T., *Numerical Recipes in FORTRAN, The Art of Scientific Computing*, Cambridge Univ. Press, Cambridge, England, U.K., 1986.

[30] Eklund, D. R., Drummond, J. P., and Hassan, H. A., "Calculation of Supersonic Turbulent Reacting Coaxial Jets," *AIAA Journal*, Vol. 28, No. 9, 1990, pp. 1633–1641. doi:10.2514/3.25262

[31] Kee, R. J., Rupley, F. M., and Miller, J. A., "CHEMKIN-II: A Fortran Chemical Kinetics Package for the Analysis of Gas-Phase Chemical Kinetics," Sandia National Labs., Rept. SAND89-8009 UC-401, Albuquerque, NM, 1989.

[32] FLUENT, Software Package, Ver. 6.2, Fluent, Inc., Natick, MA, Feb. 2005.

[33] Jones, W. P., and Mussonge, P., "Closure of the Reynolds Stress and Scalar Flux Equations," *Physics of Fluids*, Vol. 31, No. 12, 1988, pp. 3589–3604.

[34] Mura, A., and Borghi, R., "Towards an Extended Scalar Dissipation

Equation for Turbulent Premixed Combustion," *Combustion and Flame*, Vol. 133, Nos. 1–2, 2003, pp. 193–196. doi:10.1016/S0010-2180(02)00565-5

[35] Mura, A., Robin, V., and Champion, M., "Modeling of the Scalar Dissipation in Partially Premixed Turbulent Flames," *Combustion and Flame*, Vol. 149, Nos. 1–2, 2007, pp. 217–224. doi:10.1016/j.combustflame.2006.11.004

[36] Vingert, L., Habiballah, M., Vuillermoz, V., and Zurbach, S., "Mascotte: A Test Facility for Cryogenic Combustion Research at High Pressure," *Proceedings of the 51st International Astronautical Congress*, Rio de Janeiro Brazil, Oct. 2000.

[37] Juniper, M., Tripathi, A., Scouflaire, P., Rolon, J. C., and Candel, S. M., "The Structure of Cryogenic Flames at Elevated Pressure," *Proceedings of the Combustion Institute*, Vol. 28, 2000, pp. 1103–1109.

[38] Cheng, G. C., and Farmer, R. C., "Development of Linearized Real Fluid Model in Simulating Spray Combustion Flows," AIAA Paper 2002-0735, Jan. 2002.

[39] Cheng, G. C., and Farmer, R. C., "Development of Efficient Real Fluid Model in Simulating Liquid Rocket Injector Flows," AIAA Paper 2003-4466, July 2003.

[40] Harstad, K., and Bellan, J., "An All-Pressure Fluid Drop Model Applied to a Binary Mixture: Heptane in Nitrogen," *International Journal of Multiphase Flow*, Vol. 26, No. 10, 2000, pp. 1675–1706. doi:10.1016/S0301-9322(99)00108-1

[41] Harstad, K., and Bellan, J., "Interactions of Fluid Oxygen Drops in Fluid Hydrogen at Rocket Chamber Pressures," *International Journal of Heat and Mass Transfer*, Vol. 41, No. 22, 1998, pp. 3551–3558. doi:10.1016/S0017-9310(98)00048-9

[42] Marble, F., and Broadwell, J. E., "The Coherent Flame Model for Turbulent Chemical Reactions," *Project Squid Headquarters*, Chaffee Hall, Purdue Univ., TR TRW-9-PU, Purdue, IN, Jan. 1977.

[43] Candel, S. M., and Poinsot, T. J., "Flame Stretch and the Balance Equation for the Flame Area," *Combustion Science and Technology*, Vol. 70, No. 1–3, 1990, pp. 1–15. doi:10.1080/00102209008951608

[44] Mura, A., and Demoulin, F. X., "A Lagrangian Intermittent Modelling for Turbulent Lifted Flames," *Combustion Theory and Modelling*, Vol. 11, No. 2, 2007, pp. 227–257.

[45] Candel, S., Herding, G., Snyder, R., Scouflaire, P., Rolon, C., Vingert, L., Habiballah, M., Grisch, F., Péalat, M., Bouchardy, P., Stepowski, D., Cessou, A., and Colin, P., "Experimental Investigation of Shear-Coaxial Cryogenic Jet Flame," *Journal of Propulsion and Power*, Vol. 14, 1998, pp. 826–834. doi:10.2514/2.5346

[46] Singla, G., Scouflaire, P., Rolon, J. C., and Candel, S. M., "Planar Laser Induced Fluorescence of OH in High Pressure Cryogenic LOx/GH2 Jet Flames," *Combustion and Flame*, Vol. 144, Nos. 1–2, 2006, pp. 151–169. doi:10.1016/j.combustflame.2005.06.015

J. Oefelein
Associate Editor